Humanized mouse model supports development, function, and tissue residency of human natural killer cells

Dietmar Herndler-Brandstetter[a,1], Liang Shan[a,1,2], Yi Yao[b,3], Carmen Stecher[a], Valerie Plajer[a], Melanie Lietzenmayer[a], Till Strowig[a,4], Marcel R. de Zoete[a,5], Noah W. Palm[a], Jie Chen[a], Catherine A. Blish[c], Davor Frleta[d], Cagan Gurer[d], Lynn E. Macdonald[d], Andrew J. Murphy[d], George D. Yancopoulos[d], Ruth R. Montgomery[b], and Richard A. Flavell[a,e,6]

[a]Department of Immunobiology, Yale University School of Medicine, New Haven, CT 06519; [b]Department of Internal Medicine, Yale University School of Medicine, New Haven, CT 06519; [c]Department of Medicine, Stanford University School of Medicine, Stanford, CA 94305; [d]Regeneron Pharmaceuticals Inc., Tarrytown, NY 10591; and [e]Howard Hughes Medical Institute, New Haven, CT 06519

Contributed by Richard A. Flavell, September 18, 2017 (sent for review March 30, 2017; reviewed by Hergen Spits and Wayne M. Yokoyama)

Immunodeficient mice reconstituted with a human immune system represent a promising tool for translational research as they may allow modeling and therapy of human diseases in vivo. However, insufficient development and function of human natural killer (NK) cells and T cell subsets limit the applicability of humanized mice for studying cancer biology and therapy. Here, we describe a human interleukin 15 (*IL15*) and human signal regulatory protein alpha (*SIRPA*) knock-in mouse on a *Rag2*$^{-/-}$ *Il2rg*$^{-/-}$ background (SRG-15). Transplantation of human hematopoietic stem and progenitor cells into SRG-15 mice dramatically improved the development and functional maturation of circulating and tissue-resident human NK and CD8^{+} T cells and promoted the development of tissue-resident innate lymphoid cell (ILC) subsets. Profiling of human NK cell subsets by mass cytometry revealed a highly similar expression pattern of killer inhibitory receptors and other candidate molecules in NK cell subpopulations between SRG-15 mice and humans. In contrast to nonobese diabetic severe combined immunodeficient *Il2rg*$^{-/-}$ (NSG) mice, human NK cells in SRG-15 mice did not require preactivation but infiltrated a Burkitt's lymphoma xenograft and efficiently inhibited tumor growth following treatment with the therapeutic antibody rituximab. Our humanized mouse model may thus be useful for preclinical testing of novel human NK cell-targeted and combinatory cancer immunotherapies and for studying how they elicit human antitumor immune responses in vivo.

humanized mice | cancer immunotherapy | IL-15 | NK cells | ILC

Cancer immunotherapy has emerged as one of the most promising therapeutic interventions to eliminate malignant diseases (1, 2). It does so by utilizing the power and specificity of the immune system, thereby reducing the severity of side effects that have been seen with chemotherapy or radiation treatment regimens. Immunotherapeutic approaches have been designed to target a variety of molecules on different cells of the immune system, including T cell subsets, natural killer (NK) cells, and myeloid cells (3–6). However, a major challenge that the cancer immunotherapy field currently faces is to identify combinations of therapeutics that will lead to complete and durable responses.

Injection of human hematopoietic stem and progenitor cells into immunodeficient mice, such as *Rag2*$^{-/-}$ *Il2rg*$^{-/-}$ (RG) or nonobese diabetic severe combined immunodeficient *Il2rg*$^{-/-}$ (NSG) mice, supports basic development of human immune cells in vivo (7, 8). As such, humanized mice represent a promising model for studying human immune function and diseases in vivo and could be used to screen and identify highly effective combinations of cancer therapeutics. However, the poor interspecies cross-reactivity of factors that are essential for the physiological and functional development of human immune cells in humanized mice highlights the need to improve the currently available humanized mice (9). One such cytokine, with only 65% of amino acids identical between humans and mice, is interleukin 15 (IL-15). IL-15 is essential for the development and/or function of NK cells, memory CD8 T cells, CD8αα intraepithelial lymphocytes (IELs), and tissue-resident NK cells (10, 11). In addition, physiological levels of IL-15 are essential for functional antitumor responses of NK and T cells in cancer immunotherapy (12). Three studies showed that hydrodynamic injection of plasmid DNA encoding human IL-15 into NSG mice, injection of human IL-15/IL-15Rα into *Rag2*$^{-/-}$ *Il2rg*$^{-/-}$ mice, or transgenic expression of IL-2 led to a transient increase of functional human NK

Significance

Humanized mice represent a promising approach to study the human immune system in health and disease. However, insufficient development and function of human lymphocytes limit the applicability of humanized mice for cancer biology and therapy. We demonstrate that human *SIRPA* and *IL15* knock-in (SRG-15) mice support efficient development of circulating and tissue-resident natural killer (NK) cells, intraepithelial lymphocytes, and innate lymphoid cell subsets. In contrast to previous humanized mouse models, human NK cells in SRG-15 mice mediate efficient antibody-dependent cellular cytotoxicity and thereby enable NK cell-targeted cancer immunotherapy of tumor xenografts. As such, SRG-15 humanized mice may facilitate translational research by enabling the development of novel NK and CD8^{+} T cell-based therapeutic approaches that target human infections and malignancies.

Author contributions: D.H.-B., L.S., Y.Y., T.S., C.A.B., and R.R.M. designed research; D.H.-B., L.S., Y.Y., C.S., V.P., M.L., T.S., M.R.d.Z., N.W.P., and J.C. performed research; D.F., C.G., L.E.M., A.J.M., and G.D.Y. contributed new reagents/analytic tools; D.H.-B., L.S., Y.Y., and T.S. analyzed data; and D.H.-B., L.S., and R.A.F. wrote the paper.

Reviewers: H.S., Academic Medical Centre of the University of Amsterdam; and W.M.Y., Washington University School of Medicine.

Conflict of interest statement: D.F., C.G., L.E.M., A.J.M., and G.D.Y. are employees and shareholders of Regeneron Pharmaceuticals. Regeneron Pharmaceuticals, D.H.-B., L.S., T.S., M.R.d.Z., N.W.P., and R.A.F. have filed a patent application related to this work.

[1]D.H.-B. and L.S. contributed equally to this work.

[2]Present address: Department of Medicine, Pathology and Immunology, and The Andrew M. and Jane M. Bursky Center for Human Immunology and Immunotherapy Programs, Washington University School of Medicine, St. Louis, MO 63110.

[3]Center for Cutaneous Biology and Immunology Research, Department of Dermatology, Henry Ford Health System, Detroit, MI 48202.

[4]Present address: Research Group Microbial Immune Regulation, Helmholtz Centre for Infection Research, 38124 Braunschweig, Germany.

[5]Present address: Department of Infectious Diseases and Immunology, Utrecht University, 3584 CL Utrecht, The Netherlands.

[6]To whom correspondence should be addressed. Email: richard.flavell@yale.edu.

This article contains supporting information online at www.pnas.org/lookup/suppl/doi:10.1073/pnas.1705301114/-/DCSupplemental.

cells (13–15). M-CSF$^{h/h}$ IL-3/GM-CSF$^{h/h}$ SIRPA$^{h/m}$ TPO$^{h/h}$ *Rag2*$^{-/-}$ *Il2rg*$^{-/-}$ (MISTRG) mice, a humanized mouse model that supports efficient development of human myeloid cells, also showed improved development of human NK cells, in particular in the liver (16). However, engrafted MISTRG mice developed anemia, which limited their lifespan. In this study, knock-in replacement of the mouse *Il15* coding sequence by the human *IL15* coding sequence had the advantage of proper expression of physiological levels of IL-15 in a tissue- and cell-specific manner, as opposed to DNA or protein injection. Engrafted SRG-15 mice showed improved functional development of circulating and tissue-resident human NK and CD8$^+$ T cells, promoted the development of innate lymphoid cell (ILC) subsets, lived for at least 9 mo, and demonstrated efficient tumor growth inhibition following NK cell-targeted cancer immunotherapy. As such, SRG-15 mice may facilitate translational research by enabling the development of novel therapeutic approaches that target human infections and malignancies.

Results

Generation of Human SIRPA and Human IL15 Knock-in Mice. Since polymorphism of the mouse signal regulatory protein alpha (*Sirpa*) modulates the engraftment of human hematopoietic stem cells (17–19), we generated a human *SIRPA* knock-in mouse, which expresses the human extracellular domain of SIRPα under the control of the mouse promotor (Fig. 1*A*). Human SIRPα was highly expressed on the surface of circulating mouse CD45$^+$ cells (Fig. 1*B*) and mouse myeloid cell subsets (Fig. S1 *A* and *B*) in nonengrafted human *SIRPA* knock-in *Rag2*$^{-/-}$ *Il2rg*$^{-/-}$ (S$^{h/h}$RG) mice. Furthermore, the expression level of human SIRPα in mouse CD45$^+$ cells of engrafted heterozygous (human/mouse) SIRPA *Rag2*$^{-/-}$ *Il2rg*$^{-/-}$ (S$^{h/m}$RG) mice was comparable with hCD45$^+$ cells (Fig. 1*C*). We next compared human immune cell reconstitution in NSG, S$^{h/m}$RG, and S$^{h/h}$RG mice 14 wk postengraftment with human CD34$^+$ hematopoietic stem and progenitor cells. While NSG and S$^{h/m}$RG mice showed similar human CD45$^+$ cell engraftment levels in the blood and bone marrow (BM), the engraftment level in S$^{h/h}$RG mice was significantly decreased (Fig. 1*D*). Since S$^{h/h}$RG mice did not express extracellular mouse SIRPα, the absence of mouse CD47-SIRPα signaling may lead to bone cell loss and may thus impair human immune cell engraftment in the mouse BM niche (20). Consequently, only heterozygous SIRPA *Rag2*$^{-/-}$ *Il2rg*$^{-/-}$ (SRG) mice were used for all subsequent experiments. Further characterization of engrafted SRG and NSG mice revealed that the composition of human immune cells in the blood was comparable (Fig. S1*C*). Similarly, the number of human CD45$^+$ cell numbers in the BM, spleen, and thymus, the number of human CD3$^+$ T cells in the lymph nodes, and human thymocyte subsets were comparable between NSG and SRG mice (Fig. S1 *D*–*F*). In summary, heterozygous human *SIRPA* knock-in mice (SRG) display human immune cell reconstitution that is similar to NSG mice.

The cytokine interleukin 15 (IL-15) has been shown to be essential for the proper development and function of NK cells and CD8αα intraepithelial lymphocytes (IELs) (10). We therefore generated a human *IL15* knock-in mouse (Fig. 1*E*) and crossed it onto an SRG background (S$^{h/m}$RG-15$^{h/m}$ = SRG-15). We found high expression of human *IL15* mRNA in the BM, liver, lung, and small intestine of nonengrafted SRG-15 mice (Fig. 1*F*). Upon injection of poly(I:C) into nonengrafted SRG

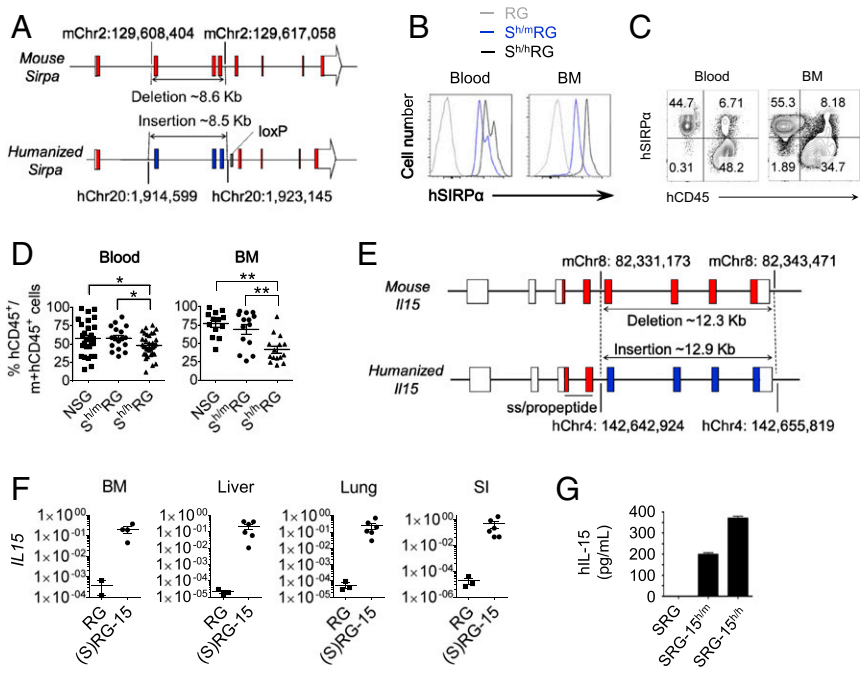

Fig. 1. Knock-in of human *SIRPA* and *IL15* in *Rag2*$^{-/-}$ *Il2rg*$^{-/-}$ (RG) mice. (*A*) Schematic representation of the targeted mouse *Sirpa* allele with human exons 2 to 4 highlighted in blue. The encoded chimeric protein has mouse signal sequence (mouse exon 1) followed by the entire human extracellular region corresponding to human amino acids 28 to 362 (human exons 2 to 4) fused to the intracellular portion of the mouse SIRPα protein (mouse exons 5 to 8) for proper signaling in mouse cells. (*B*) Expression of human SIRPα protein in mouse CD45$^+$ cells. One of three mice per group is shown. (*C*) Expression of human SIRPα protein in mouse and human CD45$^+$ cells from engrafted S$^{h/m}$RG mice. One of three mice per group is shown. (*D*) Percentage of human CD45$^+$ cells in the blood and bone marrow of NSG, S$^{h/m}$RG, and S$^{h/h}$RG mice 14 wk postengraftment. (*E*) Schematic of the targeted mouse *Il15* allele with human exons 5 to 8 highlighted in blue. The encoded chimeric protein preserves mouse signal sequence/propeptide (mouse exons 1 to 4) for proper processing in the endoplasmic reticulum and fully mature human IL-15 protein (human exons 5 to 8). (*F*) Relative expression of human *IL15* mRNA in the bone marrow, liver, lung, and small intestine (SI) of nonengrafted RG and (S)RG-15 mice. *Hprt* was used as a housekeeping gene. (*G*) Human IL-15 protein measured in the serum of SRG-15 mice following poly(I:C) treatment (n = 2 to 4 mice). Mean ± SEM are shown. *P < 0.05, **P < 0.01 (unpaired, two-tailed Student's t test).

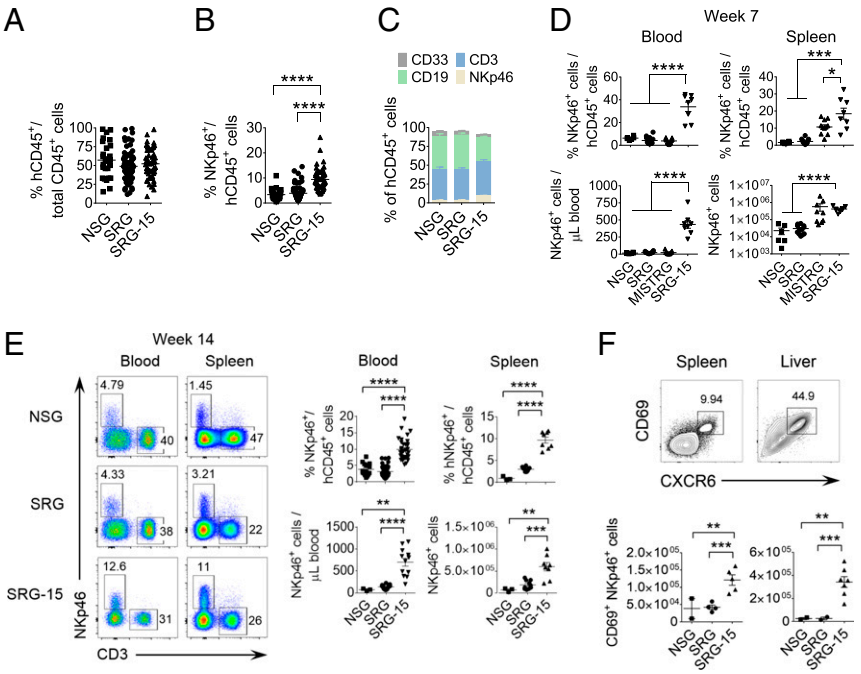

Fig. 2. Efficient development of circulating and tissue-resident human NK cells in SRG-15 mice. (*A*) Efficient engraftment of human hematopoietic cells in the blood of NSG ($n = 27$), SRG ($n = 78$), and SRG-15 mice ($n = 56$) 11 to 14 wk postengraftment with hCD34$^+$ cells. (*B*) Frequency of human NK cells in the blood of NSG, SRG, and SRG-15 mice 11 to 14 wk postengraftment. (*C*) Composition of hCD45$^+$ cells in the blood of NSG ($n = 27$), SRG ($n = 78$), and SRG-15 mice ($n = 56$) 11 to 14 wk postengraftment. (*D*) Frequency of human NK cells in the blood and spleen of NSG ($n = 6$), SRG ($n = 12$), MISTRG ($n = 11$), and SRG-15 ($n = 8$) 7 wk postengraftment. (*E*) Frequency of human NK cells in the blood and spleen of NSG ($n = 3$), SRG ($n = 10$), and SRG-15 mice ($n = 8$) 14 wk postengraftment. (*F*) Phenotype and number of CD69$^+$ tissue-resident NKp46$^+$ CD3$^-$ cells in the spleen and liver of NSG, SRG, and SRG-15 5 mo postengraftment. Mean ± SEM are shown. *$P < 0.05$, **$P < 0.01$, ***$P < 0.001$, ****$P < 0.0001$ (unpaired, two-tailed Student's *t* test).

and SRG-15 mice, human IL-15 protein was detected in the serum of heterozygous and homozygous human *IL15* knock-in mice (Fig. 1*G*).

Efficient Development of Circulating and Tissue-Resident Human NK Cells in SRG-15 Mice. To assess the impact of human IL-15 on human immune cell development, we first compared human CD45$^+$ cell engraftment between NSG, SRG, and SRG-15 mice (heterozygous human *IL15*). Human CD45$^+$ cell engraftment in the blood (Fig. 2*A*), BM, spleen, lymph node (LN), and thymus was similar between the different humanized mouse strains (Fig. S2 *A* and *B*). However, we noticed a higher percentage of human NK cells in the blood of SRG-15 mice compared with NSG and SRG mice (Fig. 2 *B* and *C*). This difference was further augmented in homozygous *IL15* knock-in mice (SRG-15$^{h/h}$) (Fig. S2*C*).

In the BM, expression of human IL-15 did not affect human pro- and pre-NK cell numbers whereas immature NK cells moderately increased (Fig. S2*D*). CD56^{bright} CD16$^-$ and CD56^{dim} CD16$^+$ mature NK cell subsets were, however, highly increased in the BM of 7-wk-old SRG-15 mice compared with NSG and SRG mice, indicating that IL-15 enhances human NK cell development, as well as survival and differentiation of mature NK cells. The number of circulating NK cells was also higher in SRG-15 mice (Fig. 2*D*) and represented physiological NK cell numbers observed in human blood [mean NK cells per microliter of blood: ∼300 (young adults), ∼400 (old adults); range: 50 to 1,200 NK cells per microliter of blood] (data from ref. 21). Although MISTRG mice have been reported to have increased human NK cells in organs, in particular in the liver (16), the number of circulating NK cells was as low as in NSG and SRG mice (Fig. 2*D*). An increased number of human NK cells were also found in the spleen of SRG-15 mice compared with NSG and SRG mice (Fig. 2*E*). In contrast to NSG and SRG mice, SRG-15 mice supported the efficient development of CD69$^+$ CXCR6$^+$ tissue-resident NK cells in the spleen and liver (Fig. 2*F*). In summary, our results show highly efficient development of circulating and tissue-resident human NK cells in SRG-15 mice.

SRG-15 Mice Promote the Development of Human ILC1 and ILC2 Subsets. Because some ILCs require IL-15 rather than IL-7 for their maintenance (22, 23), we analyzed the frequency of human ILC subsets in various organs of SRG-15 mice. Lin$^-$CD45$^+$CD7$^+$ CD127$^+$ cells in the spleen, liver, and lung rarely expressed Eomesodermin (EOMES), suggesting that these cells are rather ILCs and not NK cells (Fig. 3). While the number of CD117$^+$ CRTH2$^-$ ILC3s was comparable between SRG-15 and NSG mice, CRTH2$^+$ ILC2s and CD117$^-$ CRTH2$^-$ ILC1s were increased in the spleen, liver, and lung of SRG-15 mice compared with NSG mice (Fig. 3).

Phenotypic and Functional Profiling of Human NK Cell Subsets in SRG-15 Mice. A major shortcoming of currently available humanized mouse models, such as NSG, is the impaired development and function of mature CD56^{dim} CD16$^+$ NK cells (24). Since preactivation with IL-15 was required to induce functionally competent NK cells (25), we evaluated the in vivo cytotoxicity of human NK cells in SRG-15 mice by injecting MHC-I–expressing Raji tumor cells and MHC-I–deficient K562 tumor cells at a ratio of 1:1 (Fig. 4*A*). After 24 h, we analyzed the abundance of the two tumor cell lines and found that MHC-I–deficient K562 tumor cells were reduced in engrafted SRG-15 mice compared with engrafted SRG and nonengrafted SRG-15 mice. These results indicate that human *IL15* knock-in mice support the development of mature and functionally competent human NK cells.

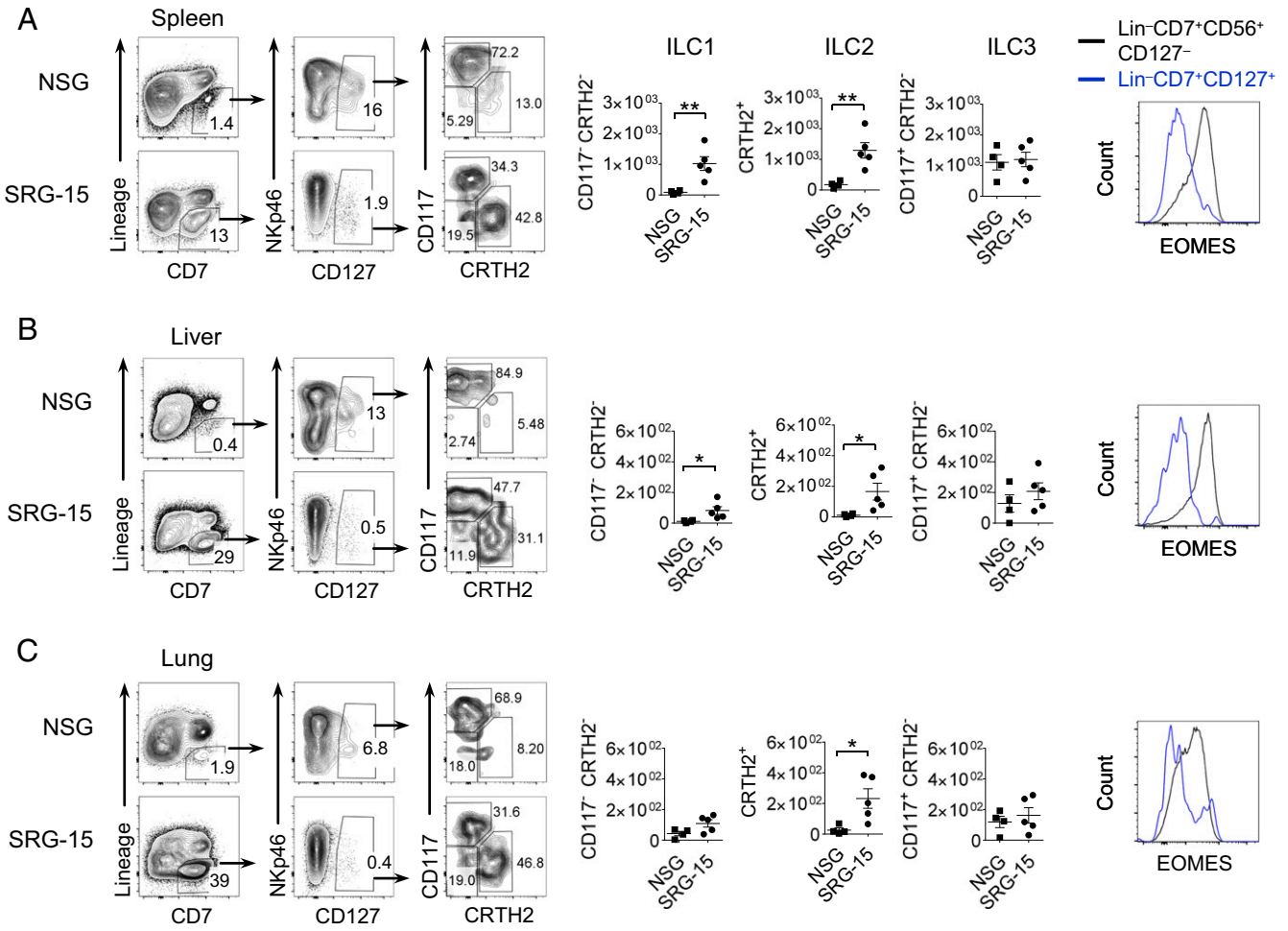

Fig. 3. SRG-15 mice support the development of human innate lymphoid cell (ILC) subsets. (*A–C*) Frequency of human ILC subsets in the spleen (*A*), liver (*B*), and lung (*C*) of NSG and SRG-15 mice 10 wk postengraftment. Total ILCs were gated on viable CD45$^+$ Lin$^-$ (CD3$^-$ CD4$^-$ CD5$^-$ TCRαβ$^-$ TCRγδ$^-$ CD14$^-$ CD19$^-$) CD7$^+$ CD127$^+$ cells (*Left*). The number of ILC1, ILC2 and ILC3 in different tissues is shown in the *Center*. The histograms (*Right*) depict the expression of EOMES in NK cells (Lin$^-$CD45$^+$CD7$^+$CD56$^+$CD127$^-$) and ILCs (Lin$^-$CD45$^+$CD7$^+$CD127$^+$) in engrafted SRG-15 mice. Mean ± SEM are shown. *$P < 0.05$ and **$P < 0.01$ (unpaired, two-tailed Student's *t* test).

In humans, two major subsets of NK cells have been identified based on the expression of CD56 and CD16 (26). Both CD56^{bright} CD16$^-$ and CD56^{dim} CD16$^+$ NK cells were present in the blood and spleen of SRG-15 mice 7 wk postengraftment (Fig. 4 *B* and *C*). In contrast, very few CD56^{bright} CD16$^-$ and CD56^{dim} CD16$^+$ NK cells were found in NSG and SRG mice. Compared with human subjects, NK cell subsets in SRG-15 mice revealed a similar distribution of CD56^{bright} and CD56^{dim} NK cell subsets and a similarly high expression of killer inhibitor receptors in the mature CD56^{dim} NK cell subset (Fig. 4 *D* and *E*).

In recent years, it has become evident that human NK cells are much more diverse than previously anticipated and are shaped by both environmental and genetic factors (27–29). To determine the phenotypic diversity of NK cell subsets that develop in SRG-15 mice, we performed a 33-parameter single-cell analysis using mass cytometry. For visualization purposes, we used viSNE, which is based on the t-Distributed Stochastic Neighbor Embedding (t-SNE) algorithm and preserves high-dimensional relationships in single-cell data collected by mass cytometry (30). Each cell is represented as a point in high dimensional space, which is based on all of the 33 parameters measured. The different colors represent high (red) or low (blue) expression of the respective molecule. Here, we focused on the mature CD56^{dim}CD16$^+$ NK cell subset because it is the dominant subset in SRG-15 mice, plays a critical role in killing of tumor cells due to its cytolytic capacity, and mediates antibody-dependent cellular cytotoxicity (ADCC) via CD16. Our results revealed a highly similar 2D distribution pattern of candidate markers in CD56^{dim}CD16$^+$ NK cells of both SRG-15 mice and humans (Fig. 4*F*). At single cell and single marker resolution, the geometric location and frequency of KIR3DL1$^+$ cells and KIR2DS4$^+$ cells, as well as NKp30$^+$CD57$^+$ PD-1$^+$ cells, among the CD56^{dim}CD16$^+$ NK cell subset were identical between SRG-15 mice and humans (Fig. 4*F*, red circles).

As the CD56^{dim}CD16$^+$ NK cell population that developed in SRG-15 mice resembled the phenotypic diversity found in human CD56^{dim}CD16$^+$ NK cells, we next analyzed the response of NK cells from SRG-15 mice and humans following stimulation with an MHC-I–deficient tumor cell line (K562) or phorbol 12-myristate 13-acetate (PMA) plus ionomycin. The geometric location [e.g., the same subset of cells that expressed high amounts of CD107a, gamma IFN (IFN-γ), and macrophage inflammatory protein (MIP)-1β] was similar in CD56^{dim}CD16$^+$ NK cells between SRG-15 mice and humans (Fig. S3*A*, red circles). Furthermore, NK cell subsets from SRG-15 mice showed a significant increase in the production of cytokines and cytotoxic molecules following stimulation with K562 or PMA plus ionomycin (Fig. S3*B*). However, stimulated NK cell subsets had a lower expression of CD107a, IFN-γ, MIP-1β, and GM-CSF in SRG-15 mice compared with humans.

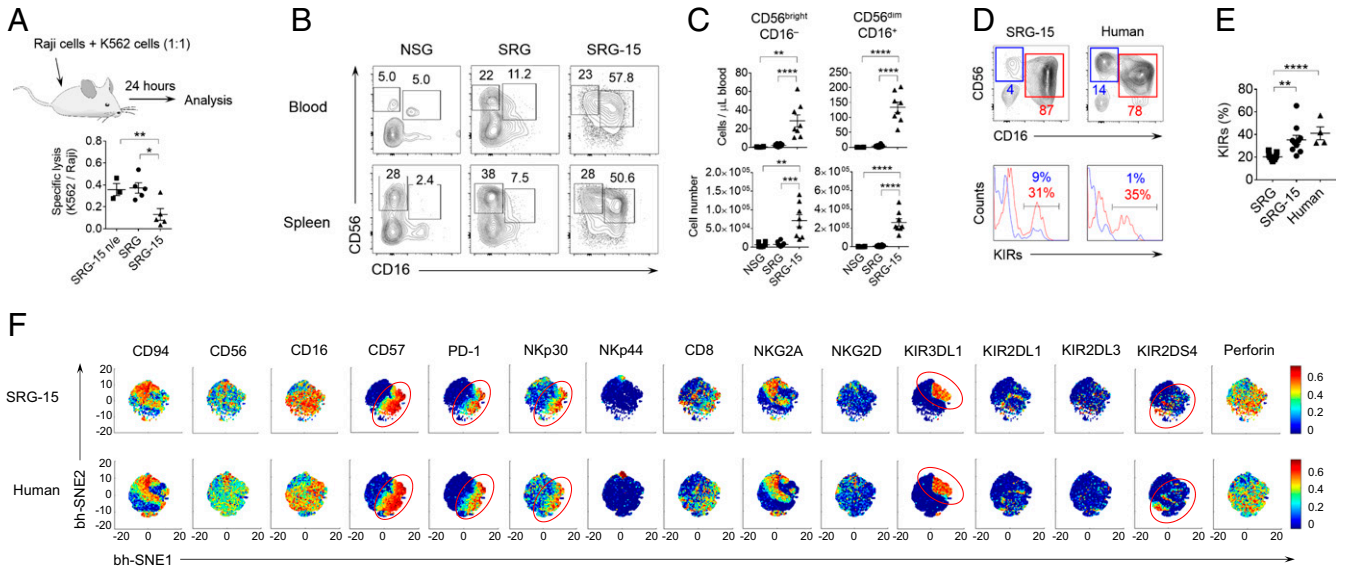

Fig. 4. Phenotypic and functional profiling of NK cells in SRG-15 mice using mass cytometry. (*A*) Human NK cells in SRG-15 mice mediated efficient in vivo killing of MHC-I–deficient K562 tumor cells but not of MHC-I–expressing Raji tumor cells. (*B* and *C*) Frequency of human CD56^{bright} CD16^{-} and CD56^{dim} CD16^{+} NK cell subsets in the blood and spleen of NSG ($n = 6$), SRG ($n = 12$), and SRG-15 mice ($n = 8$) 7 wk postengraftment with human CD34^{+} cells. (*D*) Expression of killer inhibitory receptors (KIRs) (KIR2DL1/L2/L3/S1/S3/S5/KIR3DL1) in circulating CD56^{bright} CD16^{-} (blue) and CD56^{dim} CD16^{+} NK cells (red) in SRG-15 mice ($n = 10$) and humans ($n = 4$). (*E*) Expression of KIRs in circulating CD56^{dim} CD16^{+} NK cells in SRG mice ($n = 5$–11), SRG-15 mice ($n = 10$), and humans ($n = 4$–22). (*F*) ViSNE single marker 2D scatter plots showing the expression level (red, high; blue, low) of 15 markers in CD56^{dim} CD16^{+} NK cells in SRG-15 mice ($n = 9$) and humans ($n = 20$). The red circles highlight a subpopulation of cells that express a similar set of markers. Mean ± SEM are shown. *$P < 0.05$, **$P < 0.01$, ***$P < 0.001$, ****$P < 0.0001$ (unpaired, two-tailed Student's *t* test).

Human Intraepithelial Lymphocytes Develop in the Small Intestine of SRG-15 Mice. Genetic deletion of IL-15 in mice not only results in NK cell deficiency but also leads to a decrease in memory phenotype CD8^{+} T cells and intestinal intraepithelial lymphocytes (10, 31). Although NSG mice supplemented with human IL-7 supported CD4 T cell survival, the maintenance of CD8 T cells was impaired (24). To assess the role of human IL-15 in CD8^{+} T cell survival and development of tissue-resident CD8^{+} T cells, we analyzed CD8^{+} T cells in the periphery and small intestine of SRG-15 mice. As described in Fig. S2*B*, the development of single-positive CD8^{+} T cells in the thymus was similar between SRG and SRG-15 mice. While the frequency of human CD8^{+} T cells and the CD8/CD4 ratio was comparable between NSG, SRG, and SRG-15 mice 7 wk postengraftment, a significant increase in CD8^{+} T cells and an increased CD8/CD4 ratio was observed in SRG-15 compared with SRG and NSG mice at 11 to 14 wk postengraftment (Fig. 5 *A* and *B*). In contrast to CD4^{+} T cells, more CD62L^{-} CD45RA^{-} effector-memory CD8^{+} T cells developed in SRG-15 mice compared with SRG mice (Fig. 5 *C* and *D*).

Isolation of the IEL population from the small intestine at steady state revealed a higher number of human CD45^{+} IELs in SRG-15 compared with SRG mice (Fig. 5*E*) while the number of lamina propria lymphocytes (LPLs) in the colon was similarly low in both mouse strains. Human CD45^{+} IELs comprised both CD3^{+} CD8^{+} IELs and NKp46^{+} CD3^{-} IELs. CD3^{+} CD8^{+} IELs were present at higher numbers in SRG-15 mice, expressed the tissue-resident markers CD69 and CD103, and lacked expression of CD8β (Fig. 5 *F* and *G*). Human NKp46^{+} CD3^{-} IELs were also present at higher numbers in SRG-15 mice, expressed CD56, CD69, CD103, EOMES, and lacked expression of CD127 and CD117 (Fig. 5 *H*–*J*), indicating that these cells are rather tissue-resident NK cells than innate lymphoid cells (ILCs) (22).

NK Cell-Targeted Cancer Immunotherapy in SRG-15 Mice. NK cells are able to induce antigen-independent immune responses against malignancies and pathogen-infected host cells without prior sensitization. In contrast to NSG mice, NK cells in SRG-15 mice were highly efficient in killing MHC-I–deficient K562 tumor cells in vivo, without prior preactivation (25) (Fig. 4*A*). In addition, NK cells have been reported to kill target cells via antibody-dependent cellular cytotoxicity (*ADCC*), which has been utilized for cancer immunotherapy. As ADCC mediated by NK cells is dependent on the expression of FcγRIII (CD16) and IL-15 is required for NK cell maturation and acquisition of cytolytic activity (32, 33), we tested whether NK cells in SRG-15 mice were able to kill tumor cells following treatment with a clinically approved therapeutic antibody.

NSG, SRG, and SRG-15 mice reconstituted with human CD34^{+} cells were s.c. injected with 5 million CD20-expressing Raji tumor cells. Upon formation of a visible tumor, the humanized mice were injected with an anti-human CD20 antibody [rituximab (RTX)] every 3 d (Fig. 6*A*). Rapid tumor growth was observed in nonengrafted SRG-15 mice, independent of treatment with RTX, while engrafted SRG and SRG-15 mice showed slower but constant tumor growth (Fig. 6*B*). Importantly, treatment of engrafted SRG-15 mice with RTX resulted in efficient tumor growth inhibition, both in volume and weight (Fig. 6 *B* and *C*). Although CD56^{dim} CD16^{+} cells were present in NSG and SRG mice, treatment with RTX only inhibited tumor growth in SRG-15 mice (Fig. 6 *D* and *E*), indicating that IL-15 was necessary for human NK cells to acquire functional competence and to mediate efficient killing of antibody-targeted MHC-I–expressing tumor cells. Although SRG-15 mice had a higher number of circulating NK cells, no significant differences in the frequency and composition of tumor-infiltrating T and NK cells was observed between SRG and SRG-15 mice (Fig. S4*A*). Similar to what has been observed in human tumors (34), CD56^{+} CD16^{-} NK cells were the prevalent NK cell population in the tumor microenvironment (Fig. S4*B*). We further demonstrate that tumor cell killing in SRG-15 mice was mediated via the Fc receptor as blockade of FcγRIII by a CD16 antibody completely

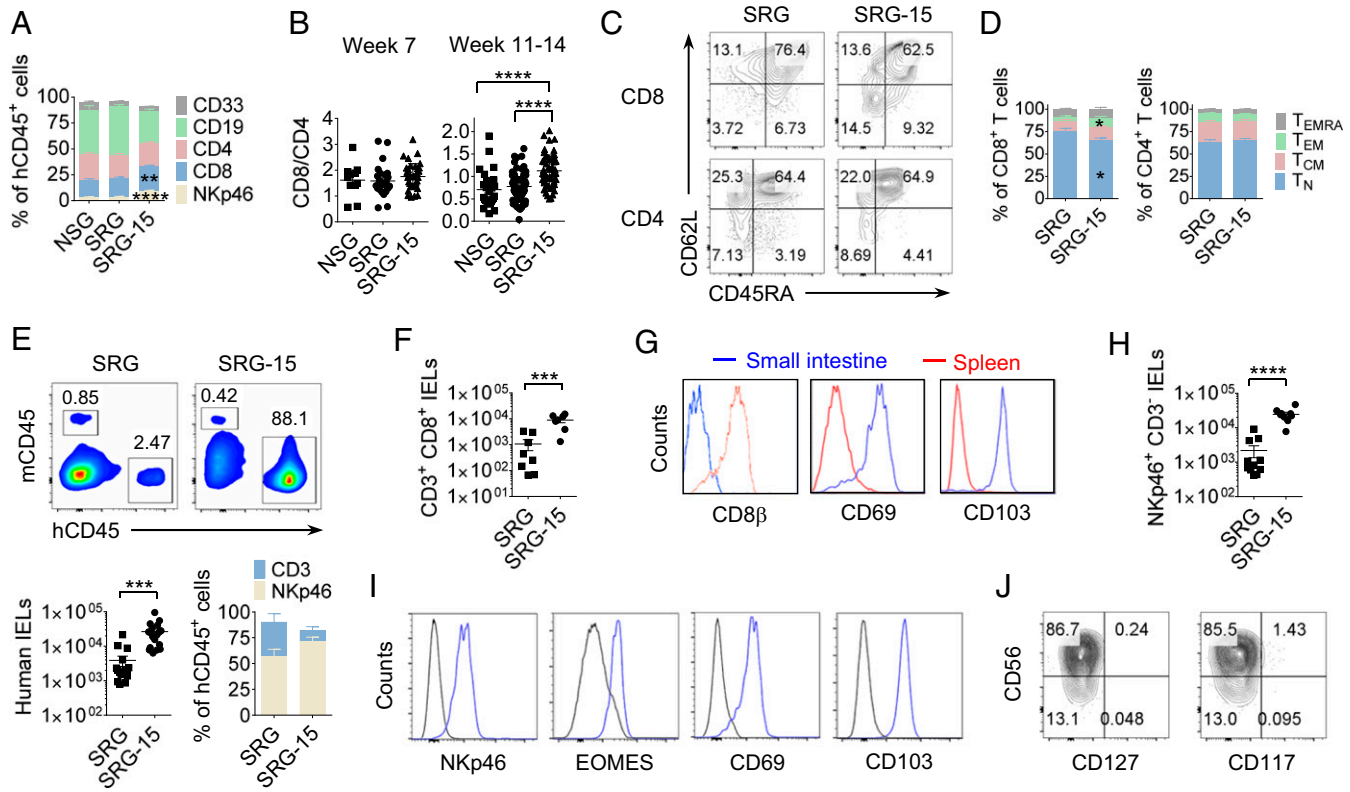

Fig. 5. Human intraepithelial lymphocytes (IELs) develop in the small intestine of SRG-15 mice. (*A*) Composition of human CD45$^+$ cells in the blood of NSG ($n = 27$), SRG ($n = 78$), and SRG-15 mice ($n = 56$) 11 to 14 wk postengraftment. (*B*) CD8/CD4 ratio in the blood of NSG ($n = 11$), SRG ($n = 26$), and SRG-15 mice ($n = 36$) 7 wk and 11 to 14 wk postengraftment (same cohort as in *A*). (*C* and *D*) Composition of human CD8$^+$ and CD4$^+$ T cells in the blood of SRG ($n = 20$) and SRG-15 mice ($n = 39$) 12 to 16 wk postengraftment. Naive (T_N), central-memory (T_{CM}), effector-memory (T_{EM}), and CD45RA$^+$ effector-memory (T_{EMRA}) T cells were defined by their expression of CD62L and CD45RA. (*E*) Percentage (*Upper*), number, and composition (*Lower*) of human CD45$^+$ IELs in the small intestine of SRG and SRG-15 mice 16 wk postengraftment. (*F*) Number of human CD3$^+$CD8$^+$ IELs in the small intestine of SRG and SRG-15 mice. (*G*) Phenotypic characteristics of CD3$^+$CD8$^+$ IELs in the spleen and small intestine of SRG-15 mice. The histograms are representative of five mice. (*H*) Number of human NKp46$^+$ CD3$^-$ IELs in the small intestine of SRG and SRG-15 mice. (*I*) Phenotypic characteristics of CD56$^+$ CD3$^-$ IELs (blue) and hCD45$^-$ cells (black) in the small intestine of SRG-15 mice. The plots are representative of six mice. (*J*) Expression of CD127 and CD117 in hCD45$^+$ IEL subsets in the small intestine of SRG-15 mice. The plots are representative of seven mice. Mean ± SEM are shown. *$P < 0.05$, **$P < 0.01$, ***$P < 0.001$, ****$P < 0.0001$ (unpaired, two-tailed Student's *t* test).

restored tumor growth in rituximab-treated SRG-15 mice (Fig. S4*C*). All three groups of SRG-15 mice had comparable engraftment levels and frequencies of human NK cells (Fig. S4*D*). The anti-human CD16 antibody efficiently blocked FcγRIII (Fig. S4*E*) and did not deplete tumor-infiltrating NK cells (Fig. S4*F*). In summary, our results demonstrate that therapeutic antibody administration induces ADCC-mediated killing of tumor cells by human NK cells in SRG-15 mice, similar to what has been observed in human patients. In contrast to NSG and SRG mice, SRG-15 mice allow efficient development and functional maturation of human NK cells and can thus be utilized as an in vivo platform for the preclinical testing of novel NK cell-targeted immunotherapies.

Discussion

Due to the lack of stromal- and epithelial-derived human IL-15, currently available humanized mice show insufficient functional development and physiological maintenance of circulating and tissue-resident human NK and CD8$^+$ T cell subsets. This severely compromises the utility of humanized mice as a preclinical model to assess human NK and CD8$^+$ T cell-based therapeutic interventions for cancer immunotherapy. We therefore developed a humanized mouse model by knock-in replacement of the coding sequence of human *IL15*. Following engraftment with human CD34$^+$ cells, SRG-15 humanized mice supported efficient development and functional maturation of circulating and tissue-resident human NK and CD8$^+$ T cell subsets and enabled human NK cell-targeted cancer immunotherapy in vivo.

In vitro studies provided evidence that IL-15 was required for the later stages of NK cell development and maturation, as well as for the acquisition of cytolytic activity (35). Similar to human cord blood, NK cells from engrafted NSG mice required preactivation by IL-15 to reach the functional competence of human adult NK cells. In particular, the terminally differentiated CD16$^+$ NK cells showed lower reactivity in the absence of IL-15 (25). In our SRG-15 mice, immature NK cells in the BM were only moderately increased while CD56^{bright} and CD56^{dim} NK cell subsets were greatly increased in tissues and the circulation. Phenotypic and functional profiling by mass cytometry confirmed that the NK cell repertoire that developed in SRG-15 mice showed a high degree of similarity to the NK cell repertoire in humans. Since NK cells can be educated by HLA class I from hematopoietic and stromal cells, knock-in replacement of mouse MHC class I by human MHC class I may further improve human NK cell education and function (36, 37), in particular, because licensed NK cell subsets play a major role in the control of MHC class I-deficient tumors, which may explain the hyporesponsiveness of human NK cell subsets stimulated with K562 in SRG-15 mice.

Expression and transpresentation of IL-15 by *Villin*-expressing intestinal epithelial cells is essential for the development and

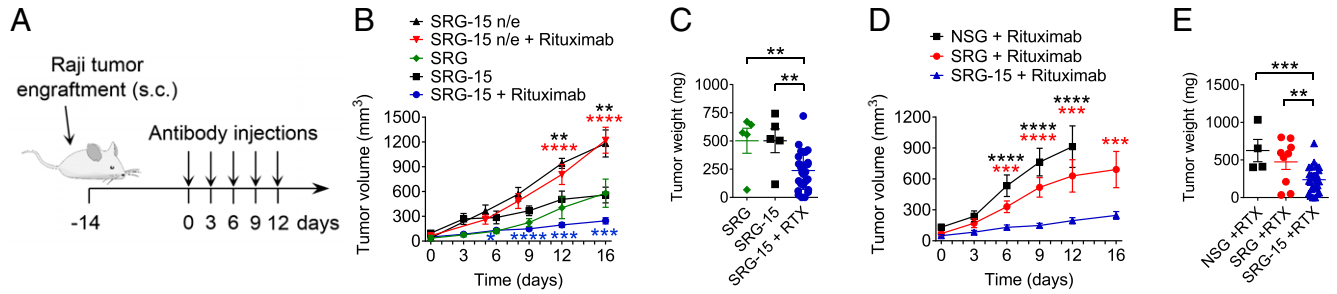

Fig. 6. NK cell-targeted cancer immunotherapy effectively inhibits tumor growth in SRG-15 but not NSG or SRG mice. (*A*) Schematic of tumor engraftment and cancer immunotherapy in humanized mice. (*B* and *C*) Rituximab (RTX) effectively inhibits tumor growth in engrafted SRG-15 mice (blue circles; $n = 28$), but not in untreated, engrafted SRG (green diamonds; $n = 5$) and SRG-15 (black squares; $n = 10$), nonengrafted (n/e) SRG-15 (black triangles; $n = 6$), and RTX-treated n/e SRG-15 mice (red triangles; $n = 4$). Significant differences: n/e SRG-15 vs. SRG-15 (black stars); RTX-treated n/e SRG-15 vs. RTX-treated SRG-15 (red stars); SRG-15 vs. RTX-treated SRG-15 (blue stars). (*D* and *E*) Rituximab effectively inhibits tumor growth in engrafted SRG-15 mice ($n = 28$), but not in NSG ($n = 4$) or SRG mice ($n = 9$). Significant differences: NSG vs. SRG-15 (black stars), SRG vs. SRG-15 (red stars). Mean ± SEM are shown. $^{*}P < 0.05$, $^{**}P < 0.01$, $^{***}P < 0.001$, $^{****}P < 0.0001$ (unpaired, two-tailed Student's *t* test).

survival of CD8$^+$ IELs and NK cells (31, 38, 39). Accordingly, human CD8αα IELs and EOMES$^+$ NK cells developed in the small intestine of SRG-15 mice and expressed the tissue-resident markers CD69 and CD103, which is consistent with findings in humans (40). Although NOD *Scid* mice transplanted with human thymus developed human IELs in the small intestine (41), these mice had progressive inflammation and sclerosis of the skin, lung, and gastrointestinal tract and developed fatal graft-versus-host disease (42). This limits the usefulness of studying IELs under physiological conditions in NOD *Scid* mice. Although IL-15 is essential for the development of circulating and tissue-resident human NK cells, it also plays a crucial role in the maintenance of tissue-resident human ILCs. Our results demonstrate that SRG-15 mice promote the development of tissue-resident CD117$^-$ CRTH2$^-$ ILC1 and CRTH2$^+$ ILC2 in various organs. SRG-15 humanized mice may therefore enable the investigation of human tissue-resident lymphoid cell differentiation and function during infections, as well as the development of immunization strategies that induce CD8$^+$ T cell-dependent mucosal immunity.

Most importantly, SRG-15 mice could be used as an in vivo platform to develop and evaluate novel strategies for cancer immunotherapy. Antibodies specifically targeting B cells, such as the anti-CD20 antibody rituximab, have been a central component in the therapy for a variety of B-cell malignancies (43). A CD16/NK cell-dependent mechanism is critical for the antibody-mediated inhibition of tumor growth in both mouse and clinical studies (44–47). In our study, human NK cells that developed in SRG-15 mice infiltrated a human tumor xenograft and inhibited tumor growth via ADCC, following treatment with rituximab. These results emphasize the functionality of human NK cells in SRG-15 mice and suggest that SRG-15 mice could be used to study NK cell-mediated immunity and cancer immunotherapy in vivo. Immune checkpoint blockade reverses exhaustion of tumor-specific T cell responses and is one of the most promising cancer immunotherapies today (48). However, in a case study of a patient with metastatic melanoma, initial tumor regression following anti–PD-1 antibody therapy was followed by acquired resistance to PD-1 therapy. This was due to a loss of MHC class I expression caused by a beta-2-microglobulin truncating mutation (49). The loss of MHC class I expression in tumor cells following anti–PD-1 antibody therapy may dramatically limit the therapeutic success of checkpoint blockade therapy and may lead to incomplete responses and subsequent disease relapse. Therefore, combination cancer immunotherapies that target both NK and CD8$^+$ T cells may be an effective strategy to overcome the loss of MHC class I in tumor cells and may achieve complete and durable responses. Since our SRG-15 mouse model supports both human NK and CD8$^+$ T cells, it could be used as a preclinical model to identify the most efficient combination of NK and CD8$^+$ T cell-based therapeutic strategies to eliminate specific tumors in vivo.

Materials and Methods

Mice. The generation of knock-in mice encoding human *SIRPA* and *IL15* in a 129xBALB/c (N3) genetic background was performed using Velocigene technology in collaboration with Regeneron Pharmaceuticals (Fig. 1 *A* and *D*). The mice were crossed to a *Rag2*$^{-/-}$ *Il2rg*$^{-/-}$ background, and human *SIRPA* and *IL15* were used as heterozygotes throughout the manuscript, until noted otherwise (Fig. 1 *D* and *G* and Fig. S2*C*), and abbreviated as follows: SRG (= S$^{h/m}$RG) and SRG-15 (= S$^{h/m}$RG-15$^{h/m}$). The humanized mice were maintained under specific pathogen-free conditions with continuous treatment of enrofloxacin in the drinking water (Baytril; 0.27 mg/mL). Nonobese diabetic (NOD) severe combined immunodeficient (*Scid*) *Il2rg*$^{-/-}$ (NSG) mice were obtained from The Jackson Laboratory. All animal studies were performed in accordance with the guidelines of the Office of Animal Research Support at Yale University.

Human Subjects. Heparinized blood from healthy volunteers was obtained after written informed consent under the guidelines of the Human Investigations Committee of Yale University School of Medicine. Purification of human peripheral blood mononuclear cells (PBMCs) was performed by density-gradient centrifugation using Ficoll-Paque (GE Healthcare) according to the manufacturer's instructions.

Human CD34$^+$ Cell Isolation and Immune Cell Reconstitution. Human CD34$^+$ cells were purified from fetal liver (FL) as described previously (16). Newborn mice received sublethal irradiation (360 cGy; X-RAD 320 irradiator), followed by intrahepatic injection of 1×10^5 human FL-derived CD34$^+$ cells. The humanized mice were bled 10 to 12 wk later, and human immune cell reconstitution was determined by flow cytometry. Only humanized mice with ≥10% human CD45$^+$ cells of total circulating CD45$^+$ cells (mouse and human CD45$^+$ cells combined) were considered successfully reconstituted and used for experiments. For experimental repeats, different donor sources of human CD34$^+$ cells were used (= independent experiments). In general, the range of variation between different donor sources was comparable with the range of variation between individual mice that were engrafted with the same donor CD34$^+$ cells.

Gene Expression Analysis. Total RNA was extracted from tissues using TRIzol reagent (Thermo Fisher Scientific) and the RNeasy Mini Kit (Qiagen). First-strand cDNA synthesis was performed using SuperScript III Reverse Transcriptase (Thermo Fisher Scientific). Quantitative reverse transcription PCR (qRT-PCR) was performed using a 7500 Fast Real-Time PCR System (Applied Biosystems) and an SYBR FAST universal qPCR kit (KAPA Biosystems). Sequence-specific oligonucleotide primers were designed using Primer3 software and synthesized by Sigma-Aldrich. The following primers were used: mouse *Hprt* forward, 5′-AGGGATTTGAATCACGTTTG-3′; mouse *Hprt* reverse, 5′-TTTACTGGCAACATCAACAG-3′; human *IL15* forward, 5′-GCCCAGGGAAATCAAAAGAT-3′; human *IL15* reverse, 5′-TGGCTCCAACAAATCAACAG-3′. Relative

expression values were calculated using the comparative threshold cycle method and normalized to mouse *Hprt*.

ELISA. Human IL-15 protein was determined by ELISA. Nonengrafted SRG, SRG-15$^{h/m}$, and SRG-15$^{h/h}$ mice were injected with 50 μg of polyinosinic-polycytidylic acid sodium salt (poly(I:C); Invivogen), and human IL-15 protein concentration was measured in the serum 18 h later using a human IL-15 Quantikine ELISA kit (R&D Systems).

Flow Cytometry. The analysis of surface molecules was performed using monoclonal antibodies from Biolegend, BD Biosciences, or eBioscience. The following anti-mouse antibodies were used: mCD11b (M1/70), mCD11c (N418), mCD45 (clone: 30-F11), mCD172a (mSIRPα; P84), Ly6C (HK1.4), and Ly6G (1A8). The following anti-human antibodies were used: CD3 (SK7 and UCHT1), CD4 (OKT4), CD5 (UCHT2), CD7 (CD7-6B7), CD8α (HIT8a and RPA-T8), CD8β (2ST8.5H7), CD10 (HI10a), CD14 (HCD14), CD16 (3G8), CD19 (HIB19), CD33 (WM53), CD34 (561), CD38 (HB-7), CD45 (HI30), CD45RA (HI100), CD56 (HCD56), CD69 (FN50), CD94 (HP-3D9), CD103 (Ber-ACT8), CD117 (104D2), CD127 (A019DS), CD158 (KIR2DL1/S1/S3/S5; HP-MA4), CD158b (KIR2DL2/L3; Dx27), CD158e1 (KIR3DL1; Dx9), CD172a (hSIRPα; SE5A5), CD294 (CRHT2; BM16), CD335 (NKp46; 9E2), EOMES (WD1928), TCRαβ (IP26), and TCRγδ (B1). Samples were acquired by an LSR II flow cytometer (BD Biosciences) and analyzed using FACSDiva (BD Biosciences) and FlowJo software.

Mass Cytometry. Marker labeling and detection were performed as described previously (50). The purified antibodies were purchased from Biolegend, BD Pharmingen, Beckman Coulter, R&D Systems, Fluidigm, Life Technologies, Abcam, or eBioscience. A single batch of metal-conjugated antibodies was conjugated in house using MaxPar X8 labeling kits according to the manufacturer's instructions (Fluidigm). The following anti-human antibodies were used: 2B4 (clone: 2-69; isotype: 165Ho), CD7 (6B7; 159Tb), CD8 (SK1; 144Nd), CD14 (M5E2; 173Yb), CD16 (3G8; 149Sm), CD19 (HIB19; 168Er), CD33 (WM53; 162Dy), CD3 (UCHT1; 147Sm), CD4 (SK3; 143Nd), CD45 (HI30; 89Y), CD56 (NCAM16.2; 174Yb), CD57 (HCD57; 145Nd), CD94 (DX22; 158Gd), GM-CSF (BVD2-21C11; 151Eu), HLA-DR (Tü36; Qdot-Cd), IFN-γ (4S.B4; 176Yb), IL-10 (JES3-9D7; 172Yb), IL-17A (BL168; 175Lu); KIR2DL1 (143211; 166Er), KIR2DL3 (180701; 170Er), KIR2DS4 (FES172; 153Eu), KIR3DL1 (DX9; 163Dy), LILRB1 (HP-F1; 154SM), MIP-1β (D21-1352; 150Nd), NKG2A (Z199; 171Yb), NKG2D (1D11; 156Gd), NKp30 (P30-15; 161Dy), NKp44 (P44-8; 169Tm), NKp46 (9E2; 155Gd), PD-1 (EH12.2H7; 146Nd), Perforin (B-D48; 167Er), and TNF-α (Mab11; 152Sm). The anti-allophycocyanin (APC) antibody (408002; 141Pr) was used to detect anti-human CD107a-APC antibody (H4A3; Biolegend). Mouse splenocytes and human PBMCs were either stimulated with 0.08 μM phorbol 12-myristate 13-acetate (PMA) and 1.3 μM ionomycin (500× cell stimulation mixture; eBioscience) or cocultured with K562 tumor cells (E:T = 10:1) for 4 h. The cells treated with PBS served as a negative control. Brefeldin A (3 μg/mL; eBioscience), Monensin (2 μM; eBioscience), and CD107a-APC antibody were added for the final 4 h of incubation for all groups. Cells were incubated with 20 mM EDTA at room temperature for 10 min before harvest. Samples were assessed by the CyTOF2 (Fluidigm) using a flow rate of 0.045 mL/min in the presence of EQ Calibration beads (Fluidigm) for normalization. All FCS files generated by CyTOF were normalized using Normalizer v0.1 MATLAB Compiler Runtime (MCR). viSNE was used for visualization of the high dimensional cytometry data into a 2D map (30).

viSNE Analysis. All FCS files generated by CyTOF were normalized using Normalizer v0.1 MCR. Gating was performed on the Cytobank platform by exclusion of debris (Iridium^{low}, DNA^{low}), multicell events (Iridium^{hi}, DNA^{hi}), and dead cells (cisplatin^{hi}) as described previously (50). After importing CyTOF data into the Matlab-based tool, cyt (30), the data were transformed using hyperbolic arcsin with a cofactor of 5. The sample size was set to 200,000 and 500,000 events with proportional sampling for CD56^{bright} and CD56^{dim} NK cells, respectively. A single viSNE run was performed on each dataset (CD56^{bright} or CD56^{dim}) generated from both SRG-15 mice and humans. The results were visualized in a 2D scatter plot (viSNE map).

Tumorigenesis. Human Raji cells (5 to 10 × 10^6) (CCL-86; ATCC) were injected s.c. into nonengrafted and hCD34$^+$-engrafted NSG, SRG, and SRG-15 mice. Upon development of a visible tumor, ~14 d postinjection, mice received i.p. injections of PBS or 100 μg of α-CD20 antibody [rituximab (RTX)] every third day. The tumor volume was determined by caliper measurement and calculated according to the following formula (51): Tumor volume (mm^3) = 0.5 × (length × width^2). Tumor-infiltrating human immune cells were isolated from the tumor xenograft using 10% FBS/RPMI 1640 supplemented with 1 mg/mL Collagenase D in a shaker for 45 min at 37 °C.

Statistical Analysis. Statistical analysis was performed using Prism 7 software (GraphPad) and two-tailed unpaired Student's *t* test.

ACKNOWLEDGMENTS. We thank Jon Alderman, Caroline Lieber, and Elizabeth Hughes-Picard for administrative assistance; Carla Weibel, Patricia Ranney, Cynthia Hughes, Elizabeth Henchey, Ann-Marie Franco, Sapna Patel, and Manjula Santhanakrishnan for mouse colony management; Stephanie C. Eisenbarth and Gabrielle Ragazzo for human blood collection; and Anthony Rongvaux and Elizabeth Eynon for discussion. D.H.-B. was supported by an Erwin Schrödinger Fellowship (Austrian Science Fund; J3220-B19). L.S. was supported by NIH Grants 1K99AI125065-01 and T32 AI07019. C.S. was supported by short-term grant abroad (KWA) scholarship (University of Vienna). V.P. was supported by a fellowship from the Austrian Marshall Plan Foundation. T.S. was supported by a fellowship from the Leukemia and Lymphoma Society. M.R.d.Z. was supported by a Rubicon Fellowship from the Netherlands Organization of Scientific Research. N.W.P. was supported by the Cancer Research Institute Irvington Fellowship Program and NIH Grant T32 AR 7107-37. Y.Y. and R.R.M. were supported by NIH Award AI 089992. This work was funded by the Bill and Melinda Gates Foundation and the Howard Hughes Medical Institute (R.A.F.).

1. Blattman JN, Greenberg PD (2004) Cancer immunotherapy: A treatment for the masses. *Science* 305:200–205.
2. Mellman I, Coukos G, Dranoff G (2011) Cancer immunotherapy comes of age. *Nature* 480:480–489.
3. Majeti R, et al. (2009) CD47 is an adverse prognostic factor and therapeutic antibody target on human acute myeloid leukemia stem cells. *Cell* 138:286–299.
4. Maloney DG, et al. (1997) IDEC-C2B8 (Rituximab) anti-CD20 monoclonal antibody therapy in patients with relapsed low-grade non-Hodgkin's lymphoma. *Blood* 90: 2188–2195.
5. Topalian SL, et al. (2012) Safety, activity, and immune correlates of anti-PD-1 antibody in cancer. *N Engl J Med* 366:2443–2454.
6. Phan GQ, et al. (2003) Cancer regression and autoimmunity induced by cytotoxic T lymphocyte-associated antigen 4 blockade in patients with metastatic melanoma. *Proc Natl Acad Sci USA* 100:8372–8377.
7. Traggiai E, et al. (2004) Development of a human adaptive immune system in cord blood cell-transplanted mice. *Science* 304:104–107.
8. Ito M, et al. (2002) NOD/SCID/gamma(c)(null) mouse: An excellent recipient mouse model for engraftment of human cells. *Blood* 100:3175–3182.
9. Rongvaux A, et al. (2013) Human hemato-lymphoid system mice: Current use and future potential for medicine. *Annu Rev Immunol* 31:635–674.
10. Kennedy MK, et al. (2000) Reversible defects in natural killer and memory CD8 T cell lineages in interleukin 15-deficient mice. *J Exp Med* 191:771–780.
11. Sojka DK, Tian Z, Yokoyama WM (2014) Tissue-resident natural killer cells and their potential diversity. *Semin Immunol* 26:127–131.
12. Waldmann TA, Dubois S, Tagaya Y (2001) Contrasting roles of IL-2 and IL-15 in the life and death of lymphocytes: Implications for immunotherapy. *Immunity* 14: 105–110.
13. Chen Q, Khoury M, Chen J (2009) Expression of human cytokines dramatically improves reconstitution of specific human-blood lineage cells in humanized mice. *Proc Natl Acad Sci USA* 106:21783–21788.
14. Huntington ND, et al. (2009) IL-15 trans-presentation promotes human NK cell development and differentiation in vivo. *J Exp Med* 206:25–34.
15. Katano I, et al. (2015) Predominant development of mature and functional human NK cells in a novel human IL-2-producing transgenic NOG mouse. *J Immunol* 194: 3513–3525.
16. Rongvaux A, et al. (2014) Development and function of human innate immune cells in a humanized mouse model. *Nat Biotechnol* 32:364–372.
17. Strowig T, et al. (2011) Transgenic expression of human signal regulatory protein alpha in Rag2-/-gamma(c)-/- mice improves engraftment of human hematopoietic cells in humanized mice. *Proc Natl Acad Sci USA* 108:13218–13223.
18. Yamauchi T, et al. (2013) Polymorphic Sirpa is the genetic determinant for NOD-based mouse lines to achieve efficient human cell engraftment. *Blood* 121: 1316–1325.
19. Takenaka K, et al. (2007) Polymorphism in Sirpa modulates engraftment of human hematopoietic stem cells. *Nat Immunol* 8:1313–1323.
20. Koskinen C, et al. (2013) Lack of CD47 impairs bone cell differentiation and results in an osteopenic phenotype in vivo due to impaired signal regulatory protein α (SIRPα) signaling. *J Biol Chem* 288:29333–29344.
21. Lin Y, et al. (2016) Changes in blood lymphocyte numbers with age in vivo and their association with the levels of cytokines/cytokine receptors. *Immun Ageing* 13:24.
22. Spits H, Bernink JH, Lanier L (2016) NK cells and type 1 innate lymphoid cells: Partners in host defense. *Nat Immunol* 17:758–764.
23. Klose CSN, et al. (2014) Differentiation of type 1 ILCs from a common progenitor to all helper-like innate lymphoid cell lineages. *Cell* 157:340–356.

24. André MC, et al. (2010) Long-term human CD34+ stem cell-engrafted nonobese diabetic/SCID/IL-2R gamma(null) mice show impaired CD8+ T cell maintenance and a functional arrest of immature NK cells. *J Immunol* 185:2710–2720.
25. Strowig T, et al. (2010) Human NK cells of mice with reconstituted human immune system components require preactivation to acquire functional competence. *Blood* 116:4158–4167.
26. Lanier LL, Le AM, Civin CI, Loken MR, Phillips JH (1986) The relationship of CD16 (Leu-11) and Leu-19 (NKH-1) antigen expression on human peripheral blood NK cells and cytotoxic T lymphocytes. *J Immunol* 136:4480–4486.
27. Horowitz A, et al. (2013) Genetic and environmental determinants of human NK cell diversity revealed by mass cytometry. *Sci Transl Med* 5:208ra145.
28. Björkström NK, Ljunggren HG, Michaëlsson J (2016) Emerging insights into natural killer cells in human peripheral tissues. *Nat Rev Immunol* 16:310–320.
29. Strauss-Albee DM, et al. (2015) Human NK cell repertoire diversity reflects immune experience and correlates with viral susceptibility. *Sci Transl Med* 7:297ra115.
30. Amir AD, et al. (2013) viSNE enables visualization of high dimensional single-cell data and reveals phenotypic heterogeneity of leukemia. *Nat Biotechnol* 31:545–552.
31. Mortier E, et al. (2009) Macrophage- and dendritic-cell-derived interleukin-15 receptor alpha supports homeostasis of distinct CD8+ T cell subsets. *Immunity* 31: 811–822.
32. Colucci F, Caligiuri MA, Di Santo JP (2003) What does it take to make a natural killer? *Nat Rev Immunol* 3:413–425.
33. Mao Y, et al. (2016) IL-15 activates mTOR and primes stress-activated gene expression leading to prolonged antitumor capacity of NK cells. *Blood* 128:1475–1489.
34. Romee R, et al. (2013) NK cell CD16 surface expression and function is regulated by a disintegrin and metalloprotease-17 (ADAM17). *Blood* 121:3599–3608.
35. Huntington ND, Di Santo JP (2008) Humanized immune system (HIS) mice as a tool to study human NK cell development. *Curr Top Microbiol Immunol* 324:109–124.
36. Landtwing V, et al. (2016) Cognate HLA absence in trans diminishes human NK cell education. *J Clin Invest* 126:3772–3782.
37. Boudreau JE, et al. (2016) Cell-extrinsic MHC class I molecule engagement augments human NK cell education programmed by cell-intrinsic MHC class I. *Immunity* 45: 280–291.
38. Burkett PR, et al. (2004) Coordinate expression and trans presentation of interleukin (IL)-15Ralpha and IL-15 supports natural killer cell and memory CD8+ T cell homeostasis. *J Exp Med* 200:825–834.
39. Ma LJ, Acero LF, Zal T, Schluns KS (2009) Trans-presentation of IL-15 by intestinal epithelial cells drives development of CD8alphaalpha IELs. *J Immunol* 183:1044–1054.
40. Sathaliyawala T, et al. (2013) Distribution and compartmentalization of human circulating and tissue-resident memory T cell subsets. *Immunity* 38:187–197.
41. Denton PW, et al. (2012) IL-2 receptor γ-chain molecule is critical for intestinal T-cell reconstitution in humanized mice. *Mucosal Immunol* 5:555–566.
42. Greenblatt MB, et al. (2012) Graft versus host disease in the bone marrow, liver and thymus humanized mouse model. *PLoS One* 7:e44664, and erratum (2013) 8:e44664.
43. Weiner GJ (2010) Rituximab: Mechanism of action. *Semin Hematol* 47:115–123.
44. Clynes RA, Towers TL, Presta LG, Ravetch JV (2000) Inhibitory Fc receptors modulate in vivo cytotoxicity against tumor targets. *Nat Med* 6:443–446.
45. Cartron G, et al. (2002) Therapeutic activity of humanized anti-CD20 monoclonal antibody and polymorphism in IgG Fc receptor FcgammaRIIIa gene. *Blood* 99: 754–758.
46. Weng WK, Levy R (2003) Two immunoglobulin G fragment C receptor polymorphisms independently predict response to rituximab in patients with follicular lymphoma. *J Clin Oncol* 21:3940–3947.
47. Treon SP, et al. (2005) Polymorphisms in FcgammaRIIIA (CD16) receptor expression are associated with clinical response to rituximab in Waldenström's macroglobulinemia. *J Clin Oncol* 23:474–481.
48. Ribas A (2012) Tumor immunotherapy directed at PD-1. *N Engl J Med* 366:2517–2519.
49. Zaretsky JM, et al. (2016) Mutations associated with acquired resistance to PD-1 blockade in melanoma. *N Engl J Med* 375:819–829.
50. Yao Y, et al. (2014) CyTOF supports efficient detection of immune cell subsets from small samples. *J Immunol Methods* 415:1–5.
51. Bullard DE, Schold SC, Jr, Bigner SH, Bigner DD (1981) Growth and chemotherapeutic response in athymic mice of tumors arising from human glioma-derived cell lines. *J Neuropathol Exp Neurol* 40:410–427.